



**HAL**  
open science

# Numerical simulation of laminar premixed hydrogen-air flame/shock interaction in semi-closed channel

Emilie Yhuel, Guillaume Ribert, Pascale Domingo

► **To cite this version:**

Emilie Yhuel, Guillaume Ribert, Pascale Domingo. Numerical simulation of laminar premixed hydrogen-air flame/shock interaction in semi-closed channel. Proceedings of the Combustion Institute, 2023, 39 (3), pp.3021-3029. 10.1016/j.proci.2022.11.002 . hal-04264907

**HAL Id: hal-04264907**

**<https://normandie-univ.hal.science/hal-04264907v1>**

Submitted on 30 Oct 2023

**HAL** is a multi-disciplinary open access archive for the deposit and dissemination of scientific research documents, whether they are published or not. The documents may come from teaching and research institutions in France or abroad, or from public or private research centers.

L'archive ouverte pluridisciplinaire **HAL**, est destinée au dépôt et à la diffusion de documents scientifiques de niveau recherche, publiés ou non, émanant des établissements d'enseignement et de recherche français ou étrangers, des laboratoires publics ou privés.

# Numerical simulation of laminar premixed hydrogen-air flame/shock interaction in semi-closed channel

Emilie Yhuel, Guillaume Ribert and Pascale Domingo  
CORIA - CNRS, Normandie Université, INSA de Rouen Normandie  
76000 Rouen, France

---

## Abstract

Highly refined simulations of flame/shock interactions (FSI) are performed and analyzed in the context of hydrogen/air combustion in a two-dimensional shock-tube configuration (height 7 cm). The chemical mechanism used for the hydrogen oxidation contains 9 reactive species, without nitrogen oxides, and 23 kinetic reactions. An initially planar laminar premixed flame ( $\phi = 0.8$ ,  $P = 20$  kPa) is left to evolve until the ratio between its burning flame velocity and the laminar flame speed reaches 1.45. Two thermal wall boundary conditions are envisaged: isothermal with  $T_{wall}$  fixed to 300 K and adiabatic. The species transport is described with a unity Lewis number for all species or by complex transport. Once the flame is established, a shock is installed in the domain which propagates toward the flame. Two values of the Mach number for the incident shock are considered:  $M_s = 1.4$  and  $M_s = 1.9$ . The relative impacts of the wall thermal condition, of the species transport modeling and of the incident shock Mach number on the FSI process are discussed. It is observed that thermal boundary conditions and transport modeling have a weak impact during the first stages of the FSI, i.e. the two successive interactions of the incoming and reflected shock with the flame, but a significant one once the reflected shock has crossed the flame front.

*Keywords:* Flame shock interaction; Hydrogen combustion; Direct Numerical Simulation

---

## 1. Introduction

The use of hydrogen as an energy carrier raises scientific questions and technological challenges as the low density of hydrogen and its propensity to explode lead to complex and dangerous use in engineering systems. Validated numerical tools are therefore essential to better predict hazardous scenarios such as the transition from low speed combustion to high speed detonation [1, 2]. In particular, the description of flame / shock interactions (FSI) is the objective of this work because it increases the flame surface, enhances the burning rate and favors the formation of detonations [3].

In the literature, fundamental studies describing the behavior of FSI are conducted in well-controlled centimetric shock-tube configurations, either numerically or experimentally [3–5]. For example, Yang and Radulescu [3] studied the interaction of a single shockwave with a stoichiometric hydrogen-air cellular flame at sub-atmospheric pressure in a Hele-Shaw shock tube configuration. A finger-type flame is first established and a planar shockwave, travelling with a Mach number  $M_s = 1.53, 1.75$  or  $1.9$ , is sent toward the flame front. Once the shockwave has passed, the flame cusps are flattened and reversed backwards into the burned gas. Richtmyer-Meshkov instabilities develop and interact with the transverse pressure waves. A classical mushroom-type flame appears far away from the initial flame location, but quickly disappears to create a finger-type flame again, but inverted [6]. In [5, 7], the incoming shockwave passes through the flame, reflects on the side wall of a channel configuration, then passes through the flame again. The role of the boundary layers appears as a keystone in the transition from a deflagration to a detonation (DDT) as in the experiment of Thomas et al. [8]. Indeed, the interaction of the reflected shock occurs with the boundary layer formed by the incident shock leading to a local oblique shock with a recirculation region. If the flame is trapped in the recirculation region, then it will be attached to the bifurcated shock and will facilitate the DDT. In [5], the flame is attached to the tail shock of the lambda structure. Finally, in [9] three-dimensional reactive Navier-Stokes numerical simulations are performed in a rectangular shock tube. Adding the third dimension affects the turbulent flame development, but has a little influence on the structure and dynamics of reactive shock bifurcations.

The majority of such simulations uses unity Lewis number approximation, adiabatic walls, one-step chemistry model in a two-dimensional configuration. The initial shape of the flame, the dimensions of the channel, the equivalence ratio of the hydrogen/air mixture [10], the incident shock Mach number are all key ingredients influencing the development of the flame inside the channel and are control parameters of the FSI. The objective of this work is to study the impact of wall boundary condition, i.e. adiabatic or isothermal, along with the trans-

port modelling assumption effects on the dynamics of the FSI in a closed tube for two values of the incident shock Mach number, using high-fidelity numerical simulations. Fully compressible reactive Navier-Stokes equations are used to simulate the unsteady FSI within the framework of the  $H_2$ /air combustion in a two-dimensional configuration.

## 2. Problem setup and numerical configuration

The cases under study correspond to lean hydrogen/air flames (equivalence ratio:  $\phi = 0.8$ ) propagating from the closed end of a two-dimensional channel and facing an incoming shockwave travelling at a Mach number  $M_s = 1.4$  or  $1.9$ . Three dimensional simulations should ideally be performed, especially to capture the boundary layer development in the transverse direction. However, a parametric study as presented in the present paper would be unaffordable in terms of cpu cost. The sketch of the configuration is given in Fig. 1. The half-height of the channel is  $h = 35$  mm and its length is  $L = 270$  mm. The wall temperature is either fixed at 300 K or prescribed based on a zero gradient relationship for temperature (adiabatic condition). A no-slip boundary condition (BC) is applied to walls and a symmetry condition is used because gravity effects can be neglected [11]. The chemical mechanism used for the hydrogen oxidation contains 9 reactive species, without nitrogen oxides, and 23 reactions in its most recent version [12]. The fully compressible Navier-Stokes equations are then solved plus 9 equations for the transport of the reactive species. In the fresh gases, the pressure (P) is set to 20 kPa as in the experiment from Yang and Radulescu [3], and the temperature is  $T = 300$  K as initial condition. Simulations are performed with the numerical code SiTCom-B. SiTCom-B is a fully compressible structured code working with cartesian grids, based on an explicit Finite Volume (FV) scheme, and has already shown its capability to predict supersonic combustion flows [13–15]. The code has a fourth-order centered skew-symmetric-like scheme for the convective terms [16] and a fourth-order centered scheme for the diffusive terms. A fourth-order RungeKutta method is applied for the time integration. Besides, second and fourth-order artificial dissipation terms of Swanson et al. [17] are implemented to overcome spurious oscillations and damp high-frequency modes. Code acceleration for the calculation of chemical source terms follows the recommendations of [18]. Either unity Lewis number for all species (notation:  $Le_1$ ) or complex transport properties (notation: CTP) have been used in the simulations presented. For the latter (CTP), mixture averaged diffusion coefficients for each species [19] are considered based on binary diffusion coefficients [20]. A correction is applied to the diffusive fluxes in order to strictly enforce mass conservation [21]. Mixture averaged viscosity [19, 22] and conductivity [23] are employed. Since the mesh resolution must ensure a proper description of the flame struc-

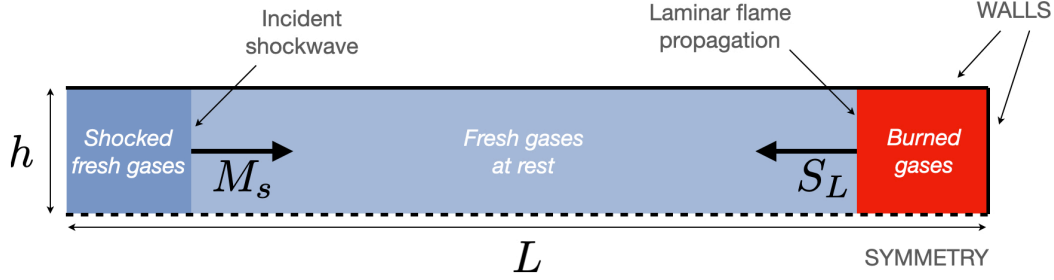


Fig. 1: Sketch of the configuration under study. The  $H_2$ /air flame propagates at  $S_L$  and the incoming shockwave moves at  $M_s = 1.4$  or  $1.9$ .  $h = 35$  mm and  $L = 270$  mm. In the fresh gases at rest,  $P = 20$  kPa,  $T = 300$  K.

ture, unstretched laminar premixed flames simulations have been performed with SiTCom-B as in [18] for various inlet conditions ( $P \in [20 - 300]$  kPa,  $T = 300$  K) and an equivalence ratio fixed to 0.8. During the establishment of the flame in the channel, 3D Navier Stokes Characteristics Boundary Conditions (NSCBC) are applied at the inlet. The results coming from SiTCom-B obtained with a mesh resolution of  $\Delta x_i = 62.5 \mu\text{m}$  match those coming from the reference code REGATH [24] for which a micrometer mesh resolution in the inner flame was employed. In Fig. 2, a comparison of the flame structure is given for  $\phi = 0.8$  and  $P = 20$  kPa. Hydrogen and oxygen decompose to mainly create  $H_2O$  and  $OH$ . The mass fraction of the latter (also  $H_2O_2$ ) exhibits a slope change (Fig. 2(b)) that is well captured by SiTCom-B, as shown in Fig. 2(d). The maximum temperature observed is 2144 K and the laminar flame speed is  $S_L = 1.79$  m/s with complex transport properties (notation: CTP) and  $S_L = 1.23$  m/s with a unity Lewis number for all species (notation:  $Le_1$ ). A resolution of  $\Delta x_i = 62.5 \mu\text{m}$  is then found adapted to capture the flame structure. However, during the FSI, this resolution might prove to be insufficient and further tests will be carried out (see section 3.1). This laminar flame structure is used as an initial condition (Fig. 1) to study the flame propagation in the two-dimensional squared channel. The results obtained with SiTCom-B are shown in Fig. 3 for an adiabatic wall BC, with a complex species transport. As already observed in the literature [10, 25, 26], the flame reorganizes itself in a "tulip" shape as it progresses towards the exit, on the left. Instabilities appear on the flame front that yield to an inhomogeneous temperature field in the burnt gases. The resulting flame shape (or surface) and location vary according to the hypothesis used: isothermal or adiabatic wall condition, unity Lewis number for all species or complex transport properties (CTP). In Fig. 4(a), the burning flame velocity,  $S_u$ ,

$$S_u = \frac{\iint_S \dot{\omega}_{Y_{H_2O}} dS}{(Y_{H_2O}^b - Y_{H_2O}^u) \rho_u h}, \quad (1)$$

normalized by  $S_L$ , is plotted as a function of time.

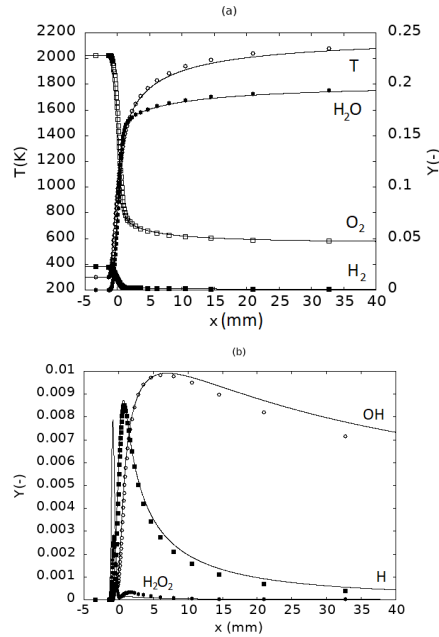


Fig. 2: Structure of an  $H_2$ /Air unstretched laminar premixed flames performed with REGATH (symbols,  $\Delta x = 1 \mu\text{m}$ ) or SiTCom-B (lines,  $\Delta x = 62.5 \mu\text{m}$ ) codes.  $H_2O_2$ :  $Y_{H_2O_2} \times 50$ .  $H$ :  $Y_H \times 5$ .

The more the flame propagates inside the channel, the more  $S_u$  increases over time due to the flame surface growth. With the adiabatic wall hypothesis, the flame progresses faster in the channel than with the isothermal BC which imposes severe heat losses to the flame leading to its extinction at the wall. Likewise, the use of a variable Lewis number allows the flame to progress more quickly. Consequently, the incident shock will interact with a flame having a structure and a position slightly different depending on the modeling hypothesis. To minimize these differences,  $S_u/S_L = 1.45$  is fixed for the three cases (adiabatic wall with CTP, fixed wall temperature with CTP, fixed wall temperature with unity Lewis number) leading to flames

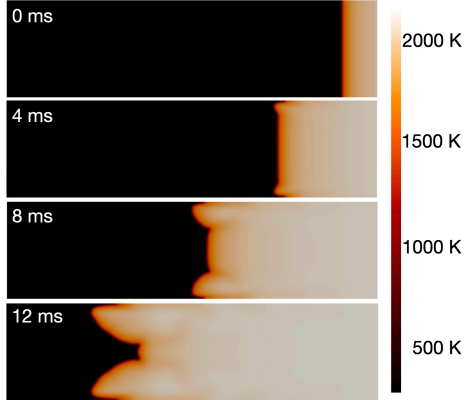


Fig. 3: Temporal evolution of an  $H_2$ /air flame ( $\phi = 0.8$ ) propagating in a two-dimensional channel with adiabatic walls, from right to left.  $P = 20$  kPa.  $\Delta x_i = 62.5 \mu\text{m}$ .

located approximately at the middle of the channel (Fig. 4(b)) at the instant where the shock is introduced inside the channel. These three flames, corresponding to three different instants but to the same ratio  $S_u/S_L = 1.45$ , will be used as the initial conditions for the study of the flame shock interaction.

### 3. Shock-flame interaction

A discontinuity in pressure and temperature is then added on the left part of the domain of simulation at 17 cm from the end wall, corresponding to a normal shock propagating from left to right at a Mach number  $M_s$  (see Fig. 1). The post-shock parameters are determined by Rankine-Hugoniot relationships. For  $M_s = 1.4$ , a temperature of  $T_s = 376$  K and a pressure of  $P_s = 42$  kPa are imposed to the shocked fresh gases; for  $M_s = 1.9$ ,  $T_s = 483$  K and  $P_s = 80$  kPa. When the shock is added, the inlet of the tube becomes a supersonic inlet at the conditions of the shocked fresh gases. From now onwards, the initial time ( $t = 0$ ) will correspond to the time of the introduction of the discontinuity inside the domain.

#### 3.1. Temporal flow evolution

In Fig. 5, a normal shock wave travels at  $M_s = 1.4$  (left) or  $M_s = 1.9$  (right) towards the flame with a weak expansion wave propagating towards the outlet, i.e. to the left. Isothermal wall boundary condition and complex transport are used.  $\Delta x_i = 31.25 \mu\text{m}$ , which corresponds to half the resolution needed for the laminar flame. The incident normal shock wave hits the flame and an increase of temperature is immediately observed ( $t = 80 \mu\text{s}$ ). The flame being initially curved, as it reaches the flame, the normal shock is exposed to various thermodynamic conditions along its surface. Consequently, the shock becomes distorted since the portion of its surface which enters first the burnt gases is accelerated. As a result

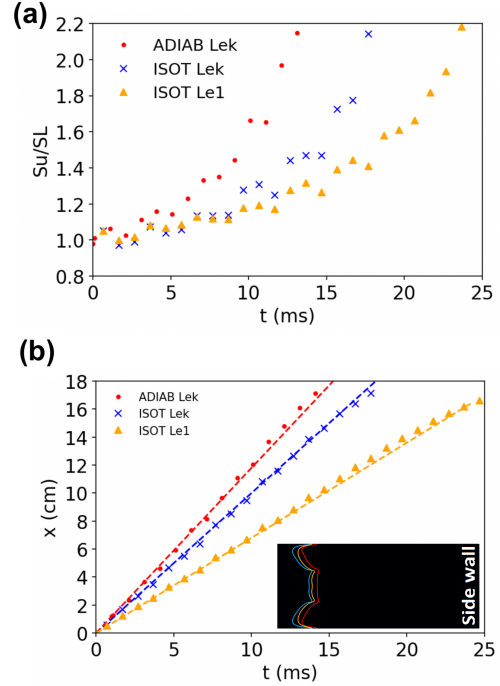


Fig. 4: (a) Burning flame velocity. (b) flame front position on the axis and flame shape for  $S_u/S_L = 1.45$  (insert).

of this first contact close to the walls, the flame surface is flattened as it is pushed toward the back wall by the shock. The pressure gradient decreases in the burnt gases, while the heat release rate increases as the shock passes through the flame front (fig. 6(b)). Once the shock has entirely crossed the flame, the whole flame front appears flattened and the flame changes its direction of propagation being pushed toward the back wall. Instabilities begin to appear near the top and bottom walls ( $t = 160 \mu\text{s}$ ). The resulting shock waves organisation gives birth to triple points which propagate in the burnt gases. Then, the shock structure and the flame progress towards the back wall. The flame begins to stretch following the arrangement of the transverse waves, and because of the high speed behind the shock wave which contrasts with the low speed in the boundary layers. The shock is reflected on the back wall between 140 and 210  $\mu\text{s}$  depending on the value of  $M_s$  and recovers a shape close to a normal shock. Then it crosses the flame front for the second time going now from burnt gases to fresh gases. The temperature in the burnt gases rises again after the reflection of the shock. During this second flame/shock interaction (between 160 and 240  $\mu\text{s}$ ), the heat release rate increases vigorously at the flame front (fig. 6(b)). Reflected pressure waves are seen behind the reflected shock wave, which from being nearly flat is starting to bend.

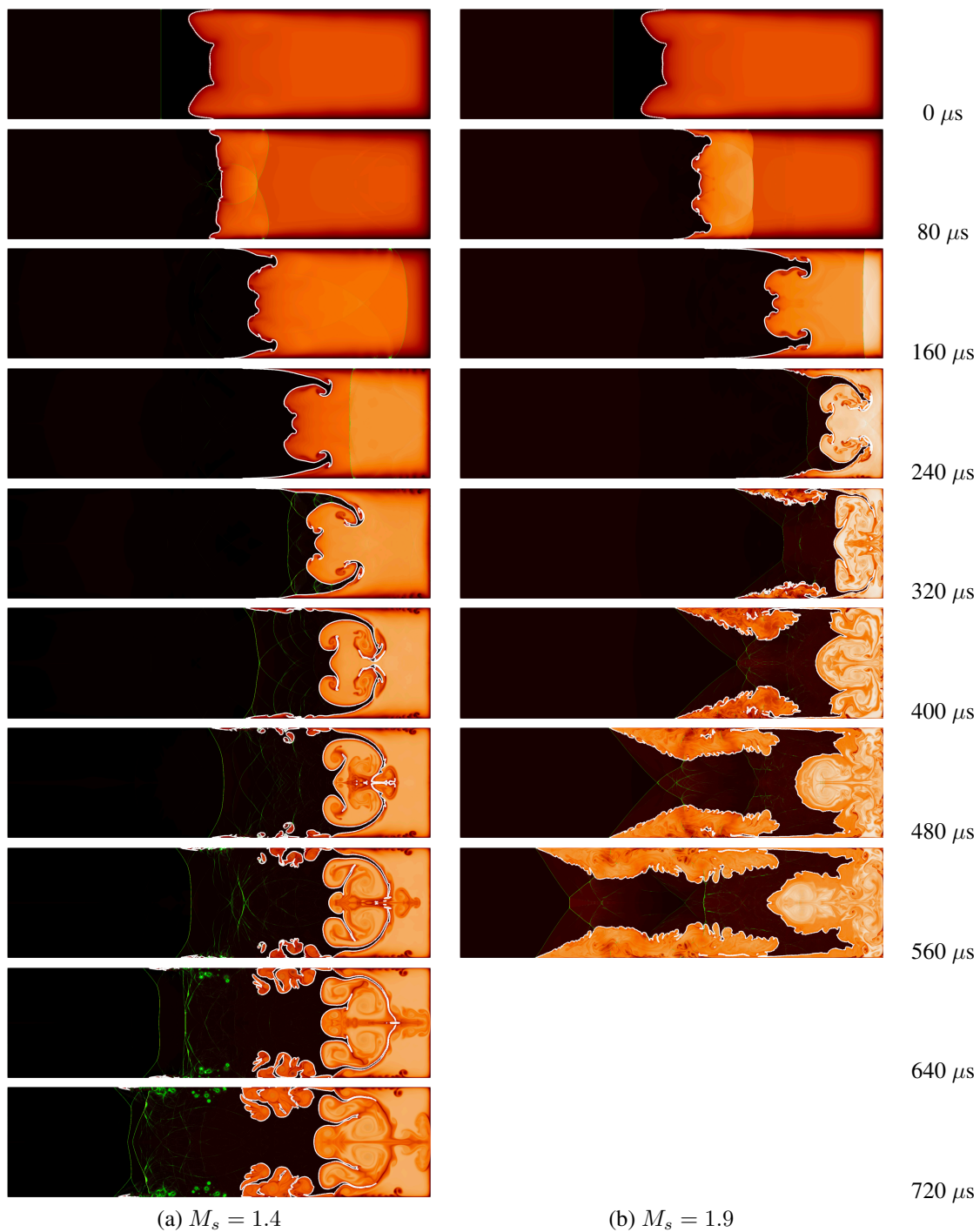


Fig. 5: Temporal flow evolution of an incident shock ( $M_s$ ) interacting with an H<sub>2</sub>/air flame. Isothermal walls, complex transport properties,  $\Delta x_i = 31.25 \mu\text{m}$ . Temperature field: black corresponds to 300 K and light orange to 3100 K. Green lines: magnitude of the pressure gradient. White line: progress variable at  $c = 0.5$ .

The flame keeps on moving towards the back wall while being the stage of Richtmyer-Meshkov instabilities. Several wave reflections are observed behind the shock and the pressure gradient increases again as it passes through the fresh gases. Around  $400 \mu\text{s}$ , the shockwave continues to propagate towards the exit, while instabilities develop with the formation of triple points due to the reflections of waves on the walls and in the instabilities. From  $320 \mu\text{s}$  for  $M_s = 1.9$  and  $400 \mu\text{s}$  for  $M_s = 1.4$ , the flame begins to display two very different behaviours: (1) the central part of the flame continues to be pushed toward the back wall and (2) the flame in the vicinity of the top and bottom walls benefits from a zone of low velocity and propagates inside the boundary layers. Eventually, the flame front becomes discontinuous and a separation occurs between the two flame regions which are now driven by different mechanism. Kelvin-Helmoltz instabilities have begun to develop in the boundary layers. The reactive shock bifurcation is clearly visible for  $M_s = 1.9$  but its intensity is much less pronounced for  $M_s = 1.4$  with flame balls detaching from it. At the end of the second shock-flame interaction temperature has increased considerably from  $2100 \text{ K}$  to  $3100 \text{ K}$  and the mean heat release has increased dramatically (factor larger than 10 for  $M_s = 1.4$  and factor larger than 100 for  $M_s = 1.9$ , Fig. 9).

The impact of the mesh resolution has been checked on the isothermal case at  $M_s = 1.9$  with complex transport (Fig. 6), through the flame surface  $S_f = \int_V |\nabla c| dV$  [27] and the mean heat release rate conditioned to  $c = Y_{H_2O}/Y_{H_2O}^{eq} = 0.5$ ,  $\text{HRR}|_{c=0.5}$ , with  $Y_{H_2O}^{eq}$  being the equilibrium value of the one-dimensional flame used for initialization. The value of  $Y_{H_2O}^{eq}$  depends essentially on the equivalence ratio which is fixed. Excepted for a few locations very close to the wall for the isothermal case, where due to the burned gases cooling a maximum value of  $c = 1.05$  has been found, the progress variable stays between 0 and 1. Around  $50 \mu\text{s}$  the incident shockwave flattens the flame front ( $S_f \searrow$ , point A) before instabilities develop and stretch the flame until the interaction of the reflected shock with the flame (B). Reactive boundary layers appear (C) and grow rapidly up to (D). Finally, the flame propagates and fills the central channel. The three mesh resolutions lead to similar results up to (C), but once the boundary layers develop, a finer mesh allows to capture the smallest structures which will control in turn the flame surface increase, i.e.  $S_f \nearrow$ . In Fig. 6(b) the different FSI steps are distinguishable again but the mesh resolution has less impact on  $\text{HRR}|_{c=0.5}$ . Instantaneous fields of temperature and pressure gradients are shown in (Fig. 6 (middle)) at  $t = 240 \mu\text{s}$ . The three meshes capture similarly the main features, but the Kelvin-Helmoltz instabilities growth in the boundary layer is totally overlooked with a  $62.5 \mu\text{m}$  mesh, which confirms the differences observed for the flame surface.

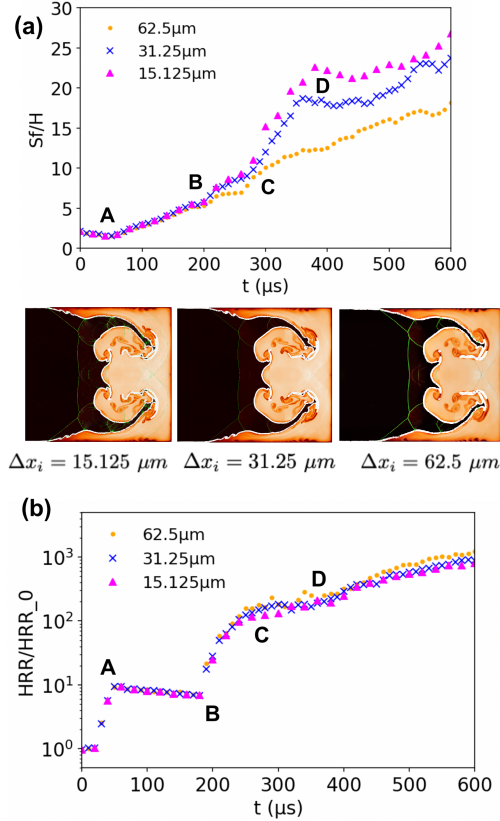


Fig. 6: Influence of the mesh resolution. Isothermal case,  $M_s = 1.9$  with CTP: (a) flame surface normalized by  $h$  ( $S_f/h$ ), Middle: temperature fields and pressure gradient at  $t = 240 \mu\text{s}$ , and (b)  $\text{HRR}|_{c=0.5}$ .

Similar trends are observed for  $M_s = 1.4$  (not shown for sake of brevity). As no noticeable differences are observed between the  $31.25 \mu\text{m}$  and the  $15.125 \mu\text{m}$  resolutions, a mesh cell of  $31.25 \mu\text{m}$  is then kept for the analysis of the results. The latter stages of the development of the reactive boundary layer (after  $400$  microseconds for the isothermal case with  $M_s$  set to  $1.9$ ) may require a finer mesh resolution as transition to turbulence is likely to occur. However, describing this transition would require a three dimensional simulation and refining further the mesh in a two-dimensional simulation would not help to better capture that transition.

### 3.2. Variable vs. unity Lewis number assumption

The simulations of the laminar flame evolving in the channel have shown a strong influence of the modeling of the species transport properties (Fig. 4). However, since the characteristic times of FSI ( $\tau_{FSI} \approx 0.03 \text{ ms}$  based on the observation of the temporal evolution of the crossing of the flame front by the shocks -incident and reflected- in the simula-

tions) are an order of magnitude less than the characteristic time of the flame ( $\tau_f = \delta_f/S_L \approx 0.2$  ms if based on  $\text{HO}_2$  radical), the impact of the diffusion of the species could therefore be neglected. This can be validated through the flame surface ( $S_f$ ) in the isothermal case for the two Mach values considered (Fig. 7). The figure 1 in Supplementary material displays the several stages of the FSI when unity Lewis number assumption is used. Compared to the evolution observed on Fig. 5, one may observe that the flame front is slightly more wrinkled when CTP are used, especially for  $M_s = 1.9$ . No significant impact is found for the first stages of the FSI (interaction with incoming and reflecting shock), however differences are clearly observed in the boundary layer development and again more pronounced for the highest Mach number. A correct description of the molecular transport allows for instabilities to develop, this observation is probably linked to the specific properties of hydrogen which is prone to thermo-diffusive instabilities, especially when the equivalence ratio is below 1. When  $M_s = 1.4$ ,  $S_f$  is more or less the same for both types of species transport properties (CTP and  $Le_1$ ). However a clear impact is observable for  $M_s = 1.9$  when  $t > 400 \mu\text{s}$ : the unity Lewis assumption hampers the development of the boundary layer compared to complex transport. The difference in behavior between the two Mach values comes from the structure of the boundary layer which is highly developed for  $M_s = 1.9$  compared to  $M_s = 1.4$  case (see fig. 5). Complex transport is then to be preferred to capture in details the whole process of the FSI in a shock-tube.

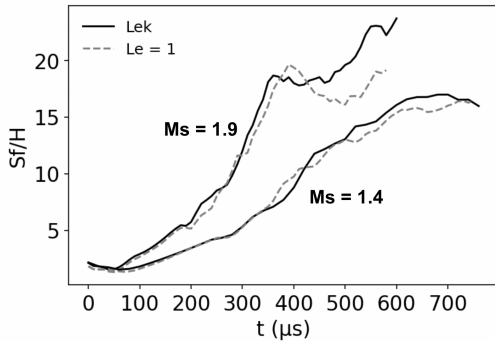


Fig. 7: Flame surface ( $S_f$ ), isothermal case -  $31.25 \mu\text{m}$ . Line: Complex Transport Properties, dashed line: unity Lewis number.

### 3.3. Influence of $M_s$ and of thermal wall BC

The influence of thermal wall boundary conditions on the flow is addressed for the two values of  $M_s$  through the temporal evolution of the total flame surface,  $S_f$  (Fig. 8),  $\text{HRR}|_{c=0.5}$  (Fig. 9), the pressure averaged in the computational domain,  $\langle P \rangle$  (Fig. 10),

and the burning flame velocity,  $S_u$  (Fig. 11). The

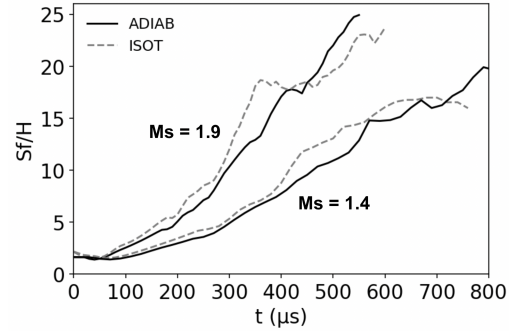


Fig. 8: Flame Surface, CTP case -  $31.25 \mu\text{m}$ .

first observation is that all these quantities dramatically increase when the incident shock Mach number,  $M_s$ , is augmented from 1.4 to 1.9, especially for  $\langle P \rangle$ ,  $\text{HRR}|_{c=0.5}$  and  $S_u$ , regardless of the wall BC. For in-

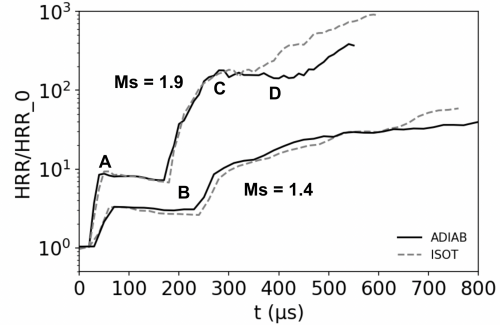


Fig. 9: Mean heat release rate conditioned to  $c = 0.5$ , CTP case -  $31.25 \mu\text{m}$ .

stance, the burning flame velocity is increased by a factor close to one thousand for Mach 1.9 and less than one hundred for Mach 1.4. This seems to indicate that increasing slightly the incident shock Mach number above 1.9 could lead to detonation.

Generally, the impact of the thermal boundary condition is found higher for the highest Mach number. The figure 2 in supplementary material displays the several stages of the FSI with adiabatic wall condition. Compared to the evolution observed on Fig. 5, one may observe that the shape of the flame is significantly modified by the change in thermal boundary condition. For the higher incident Mach number ( $M_s = 1.9$ ), the impact of the thermal boundary condition on  $S_f$ ,  $\text{HRR}|_{c=0.5}$ ,  $\langle P \rangle$  and  $S_u$  remains weak until  $300 \mu\text{s}$  (point C in Fig. 9) before getting significant.  $\langle P \rangle$  being clearly higher for the isothermal condition explains why the mean heat release rate is affected by the modification of the boundary condition for  $M_s = 1.9$ . Around  $400 \mu\text{s}$  for the adiabatic case, the reactive boundary layer becomes split increasing

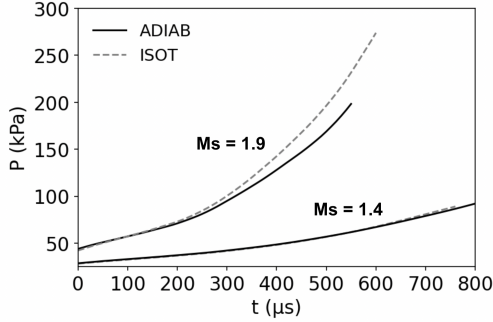


Fig. 10: Mean pressure in the computational domain, CTP case -  $31.25 \mu\text{m}$ .

the flame surface which becomes then higher than for the isothermal case. For  $M_s = 1.4$ , the impact of the thermal boundary condition is much less pronounced excepted for the flame surface after  $400 \mu\text{s}$ .

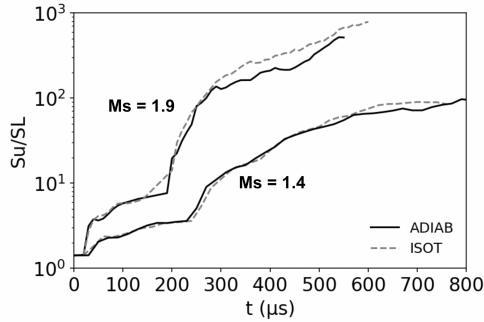


Fig. 11: Burning flame velocity, CTP case -  $31.25 \mu\text{m}$ .

These observations suggest that, even if the impact of the thermal boundary condition stays moderate for the first two interactions of the flame with the incident and reflected shock, a boundary condition as close as possible to the experiment is essential to reproduce in details the phenomena.

### 3.4. Reactive shock bifurcation

The flame anchoring mechanism in the boundary layer has been well described in [7]. When the reflected shock interacts with the reacting boundary layer, a lambda shock forms along with a recirculation region just behind it, in which the flame develops, anchors and becomes turbulent. This mechanism is clearly observed for  $M_s = 1.9$  (see Figs. 5 and 12) and whatever the thermal BC). These close-up at the edge of the boundary layer allows for visualising the difference of structure between isothermal and adiabatic condition, the latter one leading to a much less turbulent boundary reactive layer. Decreasing the incident shock Mach number to  $M_s = 1.4$  (Figs. 5 and 13) leads to a thinner and even broken reactive boundary layer. The lambda shock is still there but weaker.

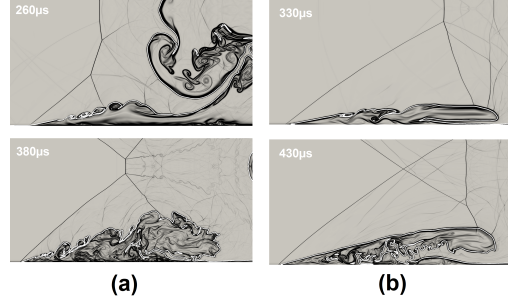


Fig. 12: Temperature gradient,  $M_s = 1.9$ : (a) isothermal and (b) adiabatic wall BC. CTP cases -  $31.25 \mu\text{m}$ .

The grid refinement becomes then crucial to capture this phenomena since for the  $62.5 \mu\text{m}$  resolution the lambda structure has not been observed.

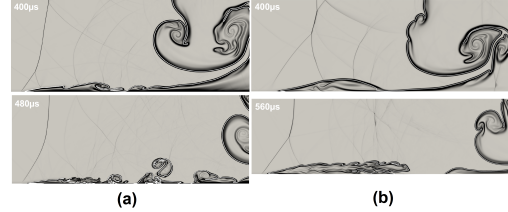


Fig. 13: Temperature gradient,  $M_s = 1.4$ : (a) isothermal and (b) adiabatic wall BC. CTP cases -  $31.25 \mu\text{m}$ .

## 4. Conclusion

Within the framework of the use of hydrogen as an energy vector, a study relating to the numerical simulation of the propagation of a laminar flame ( $\phi = 0.8$ ,  $P = 20 \text{ kPa}$ ) in a channel and interacting with a normal shockwave ( $M_s = 1.4$  and  $M_s = 1.9$ ) is proposed. A detailed kinetics mechanism is employed and the impact of the incident shock Mach number, thermal boundary condition and modeling of the species transport on the FSI has been discussed. The main observations from previous work are retrieved [3, 5–7, 9]: deformation of the flame by the incident and reflected shocks, the apparition of the Richtmyer-Meshkov instabilities, development of reactive boundary layers allowing the combustion for efficiently propagating in the fresh gases accompanied by a lambda shock, especially when the Mach number of the incident shock get close to 2. It has been demonstrated that the influence of the species transport and wall thermal conditions is significant and should be accounted for in particular in the last stage of the FSI where the reactive boundary layer strongly develops. If a predictive simulation of a real device is to be performed all these modeling assumptions have to be well designed. In this work, it has been chosen a specific initial flame front which corresponds to the transition from a pla-

nar flame to a tulip flame. Depending on the ignition device in the shock tube, several shapes could be expected at the first instant of the FSI (finger glove shape, spheric or ovoid shapes, ...). This ingredient has then to be well controlled in the experimental set-up and accurately reproduced in the initialization of the simulations.

### Acknowledgments

Emilie Yhuel is funded by the Agence Nationale de la Recherche (ANR-20-CE05-0014 - PHYSSA.) This work was performed using HPC resources from GENCI-IDRIS (Grant 2021-A0112B00152) and from CRIANN (Centre Régional Informatique et d'Applications Numériques de Normandie).

### Supplementary material

Supplementary material has been submitted.

### References

- [1] E. Oran, Understanding explosions - from catastrophic accidents to creation of the universe, *Proc. Combust. Inst.* 35(1) (2015) 1–35.
- [2] J. Shepherd, Detonation in gases, *Proc. Combust. Inst.* 32(1) (2009) 83–98.
- [3] H. Yang, M. Radulescu, Dynamics of cellular flame deformation after a head-on interaction with a shock wave: reactive richtmeyer-meshkov instability, *J. Fluids Mech.* 923 (2021).
- [4] X. Li, H. Xiao, Q. Duan, J. Sun, Numerical study of premixed flame dynamics in a closed tube : Effect of wall boundary condition, *Proc. Combust. Inst.* 38 (2021) 2075–2082.
- [5] H. Yang, M. Radulescu, Enhanced DDT mechanism from shock-flame interactions in thin channels, *Proc. Combust. Inst.* (3)38 (2021) 3481–3495.
- [6] E. Oran, V. Gamezo, Origins of the deflagration-to-detonation transition in gas-phase combustion, *Combust. Flame* 148 (2007) 4–47.
- [7] V. Gamezo, A. Khokhlov, E. Oran, The influence of shock bifurcations on shock-flame interactions and DDT, *Combust. Flame* 126 (2001) 1810–1826.
- [8] G. Thomas, R. Bambrey, C. Brown, Experimental observations of flame acceleration and transition to detonation following shock-flame interaction, *Combust. Theory Model.* 5 (2001) 573–594.
- [9] V. Gamezo, E. Oran, A. Khokhlov, Three-dimensional reactive shock bifurcations, *Proc. Combust. Inst.* 30 (2005) 1841–1847.
- [10] H. Xiao, R. Houim, E. Oran, Formation and evolution of distorted tulip flames, *Combust. Flame* 162 (2015) 4084–4101.
- [11] K. Bioche, A. Pieyre, G. Ribert, F. Richecoeur, L. Vervisch, The role of gravity in the asymmetry of flames in narrow combustion chambers, *Combust. Flame* 203 (2019) 238–246.
- [12] <<https://web.eng.ucsd.edu/mae/groups/combustion/mechanism.html>>.
- [13] L. Bouheraoua, P. Domingo, G. Ribert, Large-eddy simulation of a supersonic lifted jet flame: Analysis of the turbulent flame base, *Combust. Flame* 179 (2017) 199–218.
- [14] U. Guven, G. Ribert, Large-eddy simulation of supersonic hydrogen/oxygen combustion: application to rocketlike igniter, *J. Propul. Power* 34 (2018) 291–307.
- [15] L. J. Ruan, P. Domingo, G. Ribert, Analysis of combustion modes in a cavity based scramjet, *Combustion and Flame* 215 (2020) 228–251.
- [16] F. Ducros, V. Ferrand, F. Nicoud, C. Weber, D. Darraçq, C. Gacherieu, T. Poinso, Large-eddy simulation of the shock/turbulence interaction, *J. Comput. Phys.* 152 (1999) 517–549.
- [17] R. Swanson, R. Radespiel, E. Turkel, On some numerical dissipation schemes, *J. Comput. Phys.* 147 (1998) 518–544.
- [18] B. Duboc, G. Ribert, P. Domingo, Hybrid transported-tabulated chemistry for partially premixed combustion, *Computers Fluids* 179 (2019) 206–227.
- [19] R. B. Bird, W. E. Stewart, E. N. Lightfoot, *Combustion Physics*, John Wiley and Sons, New York, 1960.
- [20] J. Hirschfelder, C. Curtiss, R. Bird, *Molecular theory of gases and liquids*, John Wiley & Sons, 1969.
- [21] T. P. Coffee, M. Heimerl, Transport algorithms for premixed, laminar steady-state flames., *Combust. Flame* 43 (1981) 273–289.
- [22] C. R. Wilke, A viscosity equation for gas mixtures., *J. Chem. Physics* 18 (1950) 517–519.
- [23] S. Mathur, P. K. Tondon, S. C. Saxena, Thermal conductivity of binary, ternary and quaternary mixtures of rare gases., *Molecular Physics* 12 (1967) 569–579.
- [24] G. Ribert, X. Petit, P. Domingo, High-pressure methane-oxygen flames. analysis of sub-grid scale contributions in filtered equations of state, *J. Supercritical Fluids* 121 (2017) 78–88.
- [25] R. Sawyer, D. Dunn-Rankin, P. Barr, Numerical and experimental study of “tulip” flame formation in a closed vessel, *Symp. Int. Combust.* 21 (1986) 1291–1301.
- [26] H. Xiao, D. Makarov, J. Sun, V. Molkov, Experimental and numerical investigation of premixed flame propagation with distorted tulip shape in a closed duct, *Combust. Flame* 159 (2012) 1523–1538.
- [27] T. Schmitt, M. Boileau, D. Veynante, Flame wrinkling factor dynamic modeling for large eddy simulations of turbulent premixed combustion, *Flow Turb. Comb.* 94 (2015) 199–217.